

See discussions, stats, and author profiles for this publication at: <https://www.researchgate.net/publication/51477629>

# One-Step Fabrication of Nanostructured Ni Film with Lotus Effect from Deep Eutectic Solvent

ARTICLE *in* LANGMUIR · AUGUST 2011

Impact Factor: 4.46 · DOI: 10.1021/la200778a · Source: PubMed

---

CITATIONS

64

READS

124

## 2 AUTHORS:



[Changdong Gu](#)

Zhejiang University

117 PUBLICATIONS 3,439 CITATIONS

[SEE PROFILE](#)



[Jiangping Tu](#)

Zhejiang University

431 PUBLICATIONS 12,459 CITATIONS

[SEE PROFILE](#)

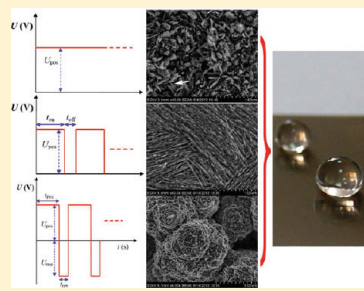
## One-Step Fabrication of Nanostructured Ni Film with Lotus Effect from Deep Eutectic Solvent

Changdong Gu\* and Jiangping Tu

State Key Laboratory of Silicon Materials and Department of Materials Science and Engineering, Zhejiang University, Hangzhou 310027, China

 Supporting Information

**ABSTRACT:** We report a procedure to fabricate nanostructured Ni films via programmed electrochemical deposition from a choline-chloride-based ionic liquid at a high temperature of 90 °C. Three electrodeposition modes using constant voltage, pulse voltage, and reverse pulse voltage produce a variety of nanostructured Ni films with micro/nanobinary surface architectures, such as nanosheets, aligned nanostrips, and hierarchical flowers. The nanostructured Ni films possess face-centered cubic crystal structure. Amazingly, it is found that the electrodeposited Ni films deliver the superhydrophobic surfaces without any further modifications by low surface-energy materials, which might be attributed to the vigorous micro/nanobinary architectures and the surface chemical composition. The electrochemical measurements reveal that the superhydrophobic Ni film exhibit an obvious passivation phenomenon, which could provide enhanced corrosion resistance for the substrate in the aqueous solutions.



### 1. INTRODUCTION

Superhydrophobic surfaces, inspired by some plants' leaves and insects' shells, share two common features: they are made of (or covered by) hydrophobic materials, and the surfaces are not flat at the micro/nanometer scales but have micro/nanobinary structures.<sup>1–7</sup> As the free metal surface is generally hydrophilic with high surface energy, the superhydrophobic pure metal surfaces are usually fabricated by the two-step approach: creating micro/nanobinary structures and chemically modifying the structured surfaces by low surface free energy materials.<sup>3–10</sup> However, it still remains a great challenge to create a superhydrophobic pure metal surface without any modification by low surface energy materials. Recently, Cao et al. fabricated a superhydrophobic pure silver surface on a copper plate without any further chemical modification, where the so-called silver flowerlike microstructure composed of nanoplates was suggested to be responsible for the superhydrophobicity of the pure metal surface.<sup>11</sup> This study implies that superhydrophobic surfaces of pure metals could be obtained by manipulating their surface topography.

Electrochemical deposition is a versatile process to fabricate metals films with micro/nanobinary structures, which have potential hydrophobic properties after chemically modifying by low surface free energy materials.<sup>4–6</sup> However, the electroplating process for hydrophobic surface fabrication is only limited to the aqueous electrolytes. Room temperature ionic liquids are superior media for the electrochemical deposition of metals and semiconductors, and have an unprecedented potential to revolutionize electrodeposition due to their wide electrochemical windows, extremely low vapor pressures, and numerous, only partly understood, cation/anion effects.<sup>12,13</sup> In particular, their negligible vapor pressures are important for minimizing the exposure to toxic volatile vapors, and their high thermal stability

(stable below 300 °C) provides a wide bath temperature range for the electrochemical synthesis under the usual atmospheric pressure. Therefore, with the substitution for traditional aqueous solvents, the electrodeposition of metals from ionic liquids should be a novel technique for the production of nanostructures due to the more control options available for ionic liquids, including the liquids themselves as well as bath temperature, voltage, and current.<sup>13–15</sup> Recently, we have demonstrated that nanoporous Ag films could be facilely deposited on copper from a choline-chloride-based deep eutectic solvent (DES), which indicated the electrochemical deposition from DES was an effective method to control the surface morphology of the deposit.<sup>7</sup> DES is a relatively new class of ionic liquid based on eutectic mixtures of choline chloride (ChCl) with a hydrogen bond donor species, which was introduced by Abbott and co-workers.<sup>16</sup> Unlike the conventional ionic liquids, DESs can be easily prepared at low cost and with high purity. Therefore, DESs are promising solvents for the deposition of a range of metal films, including Zn, Cr, and Cu, at high current efficiency.<sup>17</sup> Following a rational way, DESs should also be interesting and qualified solvents for the electrochemical synthesis of nanostructured metals or alloys with superhydrophobic surfaces.

Nickel and its alloys are some of the important engineering metallic materials, which have been attracting intensive interest due to their high hardness and good corrosion resistance.<sup>18,19</sup> The electrodeposition of a Ni film was demonstrated using a solution of the metal chloride salt in the eutectic based ionic liquids.<sup>20,21</sup> Furthermore, the nanocrystalline Ni film with a very

Received: March 1, 2011

Revised: June 4, 2011

Published: July 08, 2011

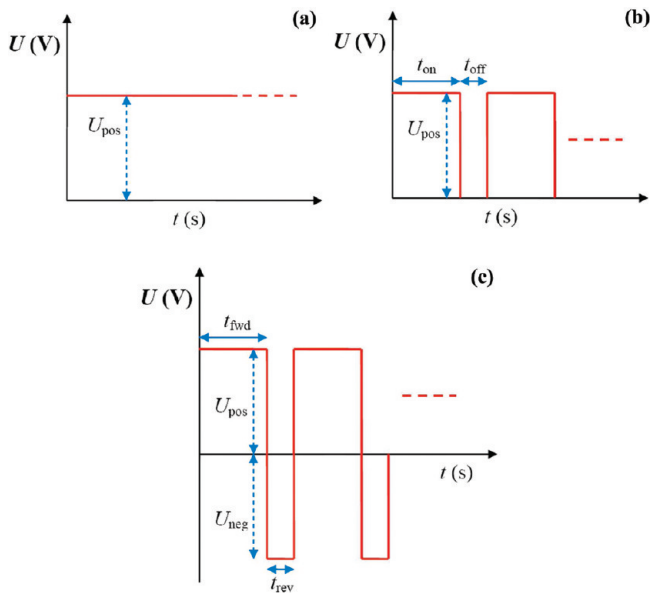


**Figure 1.** Scheme of the electrodeposition procedure. (a) Constant voltage mode (CVM),  $U_{\text{pos}} = -1.0 \text{ V}$ ; (b) pulse voltage mode (PVM),  $U_{\text{pos}} = -1.0 \text{ V}$ ; (c) reverse pulse voltage mode (RVM),  $U_{\text{pos}} = -1.0 \text{ V}$ ,  $U_{\text{neg}} = 1.0 \text{ V}$ .

high hardness of about 7.6–9.7 GPa and a good corrosion resistance was successfully electrodeposited from the ChCl-based DES at room temperature,<sup>22</sup> which may have implications in the high performance metal coatings. In this study, the so-called programmed electrodeposition procedure was carried out in the ChCl-based DES at a relatively high temperature of 90 °C, which is usually impossible to be performed for the electrodeposition in aqueous electrolytes. The procedure proposed here is to explore a one-step method to fabricate superhydrophobic metal surfaces.

## 2. MATERIALS AND METHODS

**Electrodeposition Procedure of Ni Nanostructures.** ChCl (AR, Aladdin) and ethylene glycol (EG) (AR, Aladdin) were used as received. The ChCl-based DES was prepared according to ref 23, which was formed by stirring ChCl and EG in a molar ratio of 1ChCl /2EG at 80 °C until a homogeneous colorless liquid was formed. The electrolyte is the 1ChCl/2EG solvent containing 1 M  $\text{NiCl}_2 \cdot 6\text{H}_2\text{O}$ . The substrate used was polished brass foil ( $\text{Cu}_{0.64}\text{Zn}_{0.36}$  alloy). A surface cleaning treatment of the brass substrate was conducted to remove the industrial oil from the surface by electrolytic degreasing and deionized water rinsing. Before the plating process, the substrate was dried with flowing air. The Ni films on the brass substrate were electroplated from the above electrolyte bath at various temperatures (room temperature to 90 °C). The deposition was carried out under unstirred conditions and in a voltage control mode. The operation of electroplating Ni film was undertaken in a two electrode cell for about 100 min. During the electrodeposition process, the anode consisted of an electrolytic nickel plate. The final deposits were sequentially rinsed with methanol and deionized water.

Three programmed electrodeposition modes were adopted in this study, which will hereafter be named as the constant voltage mode (CVM), the pulse voltage mode (PVM), and the reverse pulse voltage mode (RVM). The direct current constant voltage supply fulfills the CVM, and the high frequency pulse supply realizes the PVM. The voltage profiles for the three electrodeposition modes are schematically shown in Figure 1. In the CVM, the applied voltage on the substrate,

$U_{\text{pos}}$ , is a constant of  $-1.0 \text{ V}$  during the electrodeposition, as indicated in Figure 1a.

As shown in Figure 1b, in the PVM, the duty cycle,  $\nu$ , is expressed as

$$\nu = \frac{t_{\text{on}}}{t_{\text{on}} + t_{\text{off}}} = \frac{t_{\text{on}}}{T} = t_{\text{on}}f \quad (1)$$

where  $t_{\text{on}}$ ,  $t_{\text{off}}$ ,  $T$ , and  $f$  are the duration time, off-time, pulse period, and pulse frequency, respectively. In this case,  $U_{\text{pos}}$  and  $f$  keep constant as  $-1.0 \text{ V}$  and  $0.05 \text{ kHz}$ , respectively. The duty cycle,  $\nu$ , is variable, which means that the duration time of pulse voltage is changing correspondingly.

As for the RVM,  $t_{\text{fwd}}$  and  $t_{\text{rev}}$  are the on-times of forward and reverse pulses, respectively. In addition, a reverse voltage,  $U_{\text{neg}}$ , is applied on the substrate. In the present investigation,  $t_{\text{fwd}} = 2 \text{ s}$ ,  $t_{\text{rev}} = 1 \text{ s}$ ,  $U_{\text{pos}} = -1.0 \text{ V}$ , and  $U_{\text{neg}} = 1.0 \text{ V}$  are adopted for the RVM.

**Characterization.** A field emission scanning electron microscope (FE-SEM, Hitachi S-4800) was employed for the observations of the film surface and an energy dispersive X-ray spectrometer (EDS) attachment was used for qualitative elemental chemical analysis. The microstructure of the cross-sectional Ni film was analyzed with a high resolution transmission electron microscope (HR-TEM, H-800). A cross-sectional TEM sample was prepared by gluing the samples face-to-face with M-Bond 610 adhesive, and sections were cut with a diamond saw. Then the sample was ground and polished to a final thickness of approximately  $5 \mu\text{m}$ . Finally, the sample was mounted to a TEM grid and ion-milled (Gantan691) at gradually decreased voltages from 4.8 to 3.2 kV until a perforation formed. The crystalline structure of the sample was studied by using an X-ray diffractometer (XRD, XPert Pro MPD) with a Cu target ( $\lambda = 1.54056 \text{ \AA}$ ) and a monochromator at 40 kV and 250 mA with the scanning rate and step being  $4^\circ/\text{min}$  and  $0.02^\circ$ , respectively. X-ray photoelectron spectroscopy (XPS) measurement was performed with a PHI-5300 ESCA multitechnique system by using a monochromatic Mg K $\alpha$  X-ray source. All core-level spectra were referenced to the C 1s neutral carbon peak at 284.8 eV. The average surface roughness ( $R_a$ ) of the Ni films and the substrate was determined by using an optical profiler (VK-9710K, Keyence). The scanning area and vertical resolution were  $93.2 \times 69.9 \mu\text{m}^2$  and 1 nm, respectively.

The static contact angle (CA), tilt angle, and hysteresis angle measurements were all performed by using a commercial instrument (SL200B, Solon Tech., Shanghai). The indicator drop images were stored via a monochrome video camera by using a PC-based control acquisition and data process. Deionized water droplets each having a volume of  $1 \mu\text{L}$  were used in the wetting tests.

The electrochemical measurements were performed on a UI502X computer-based electrochemical analyzer (LabNet, China), which was controlled by a computer and supported by software. Linear sweep voltammetry experiments were carried out in a 3 wt % NaCl aqueous solution using a classic three-electrode cell with a platinum plate (Pt) as counter electrode and a saturated calomel electrode (SCE, +245 mV vs SHE) as reference. Potentiodynamic curves were recorded by sweeping the electrode potential from a value of about 300–400 mV lower to a value of 500–1000 mV greater than the corrosion potential, at a sweeping rate of 5 mV/s. The open circuit potential (OCP) measurements of electrodeposited Ni film and brass substrate were performed in 3 wt % NaCl solution at room temperature.

## 3. RESULTS AND DISCUSSION

**3.1. Surface Morphology.** Figure 2a and b gives the SEM images of the as-deposited Ni film by the CVM at a bath temperature of 90 °C. It is found that a highly rough surface is obtained at 90 °C, which is largely distinguished from the smooth Ni surface obtained by the same deposition parameters but at room temperature.<sup>22</sup> The rough Ni film is composed by

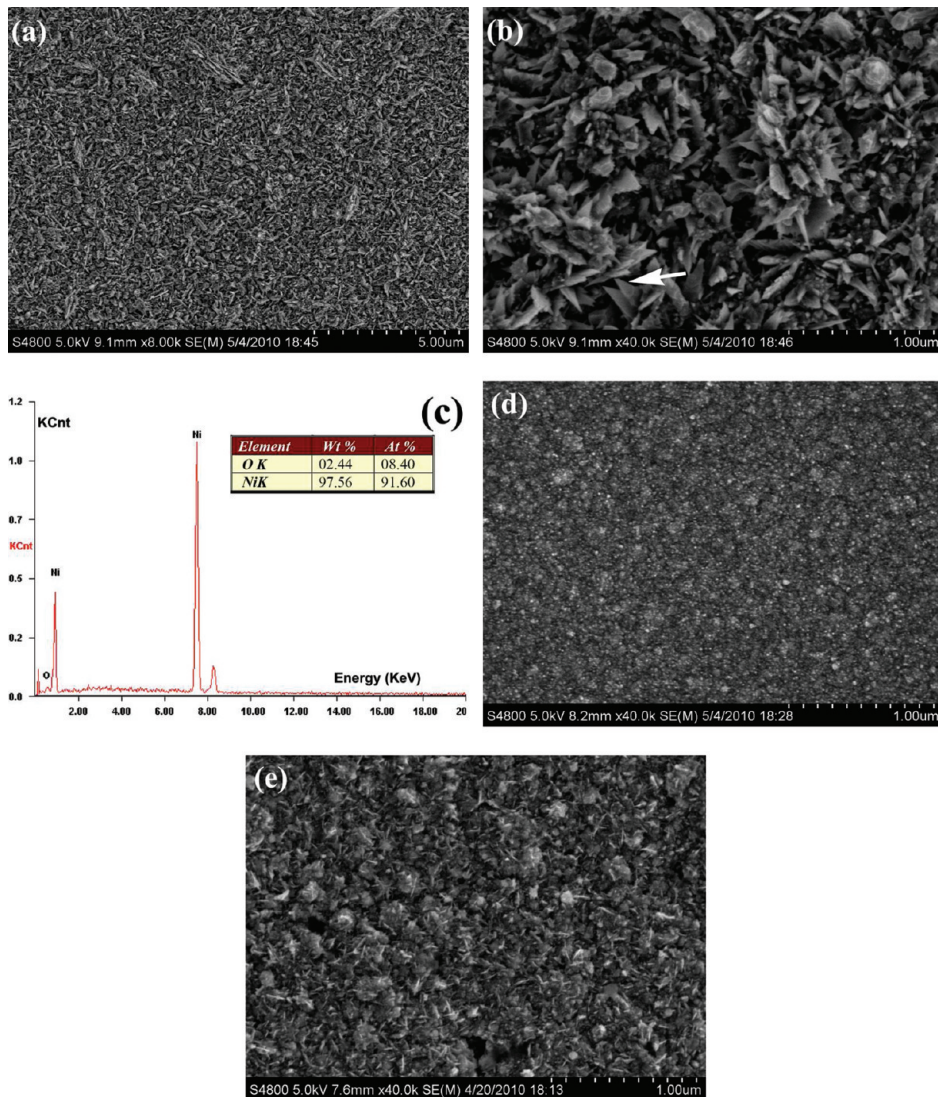


**Figure 2.** SEM images and EDS analysis of the as-deposited Ni films by the CVM at various bath temperatures. (a, b) At 90 °C; (c) EDS mapping analysis corresponding to (a); (d) at room temperature;<sup>22</sup> (e) at 60 °C.

randomly distributed Ni nanosheets with thicknesses of 10–20 nm and the 10–50 nm sized Ni grains. Furthermore, most of the Ni nanosheets exhibit arrowhead-like terminals, as indicated in Figure 2b, and are decorated by nanosized Ni grains on them. For comparison, the SEM images of the Ni films electrodeposited by the CVM at room temperature and at 60 °C were presented as Figure 2d and e, respectively. The room temperature sample shown in Figure 2d is the same as the one that appears in ref 22, which is composed by ~6 nm sized Ni grains. Clearly, it can be found that the average surface roughness ( $R_a$ ) of the Ni films increases with increasing the bath temperature, which is measured to be 0.066, 0.120, and 0.171  $\mu\text{m}$  corresponding to the bath temperature of room temperature, 60, and 90 °C, respectively. The present result indicates that the bath temperature plays an important role in manipulating the surface topography of the deposits in the ionic liquid electrodeposition. High temperature can decrease the viscosity of the ionic liquid and increase ion species mobility, which would favor the Ni nucleation and deposition process. Figure 2c gives the EDS mapping analysis corresponding to Figure 2a, which indicates that the film

is mainly composed of Ni (97.56 wt %) and the residually small amount of O species. The oxygen might be from the partial oxidation of the Ni nanocrystals.

Interestingly, when we kept the bath temperature at 90 °C and switched the electrodeposition mode from the CVM (Figure 1a) to the PVM (Figure 1b), duty cycle dependent surface morphology of Ni films was observed, as shown in Figure 3. Under the duty cycle of 10%, the fingerprint-like Ni film surface is observed as shown in Figure 3a and b. Each fingerprint-like cell with a diameter of about 3–4  $\mu\text{m}$  is composed by numerous aligned Ni strips with the length of about 1–10  $\mu\text{m}$  and the thickness of less than 20 nm. As the duty cycle increases to 30%, the aligned Ni strips as shown in Figure 3b become short and small. From the magnified SEM image (Figure 3d), it is obvious that the short aligned Ni strips are nanosheets with a thickness of about 10 nm vertically sticking on the underneath deposits. The underneath Ni deposits also possess cell structures with the diameter of about 1–2  $\mu\text{m}$ . The cell structures are decorated by nanosized nubbles to constitute a micro/nanobinary surface morphology. Further increasing the duty cycle to 50%, the nanosheets lose the aligned

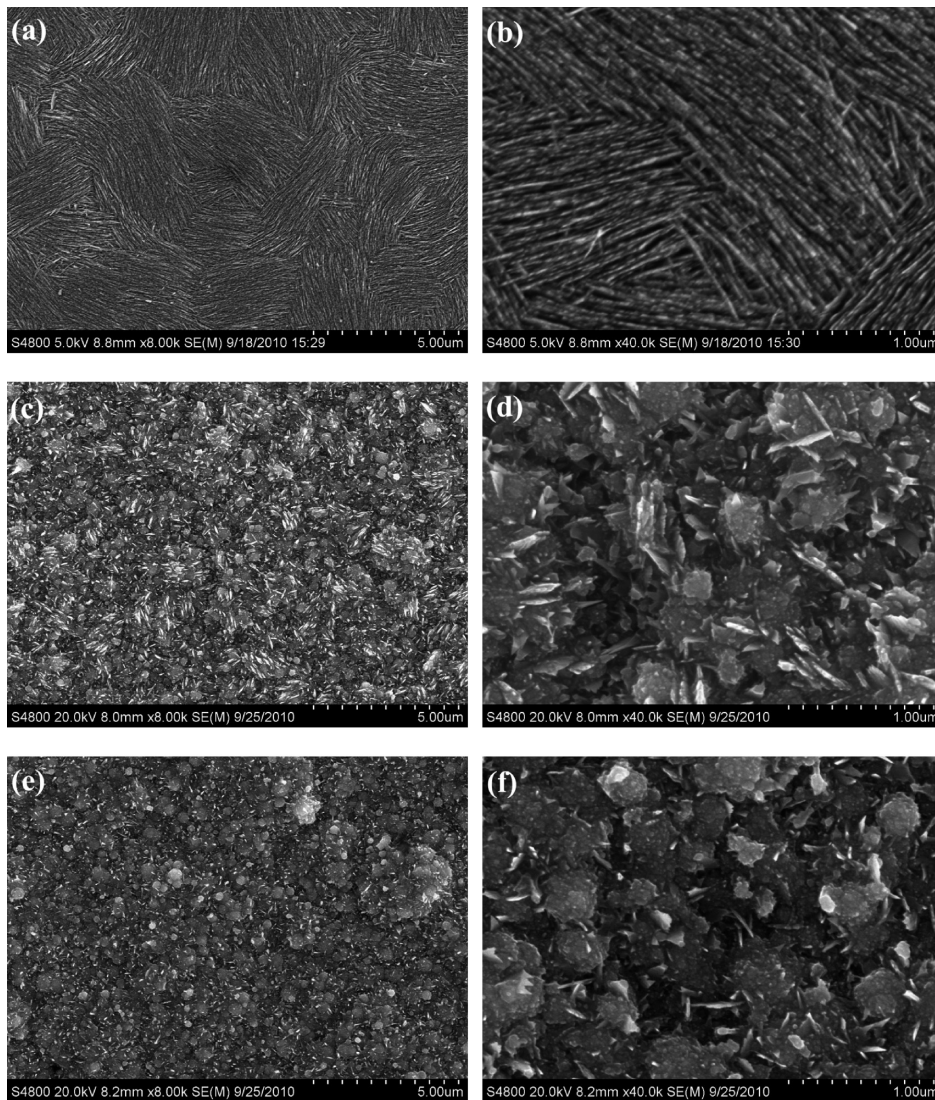


**Figure 3.** Duty cycle,  $\nu$ , dependent surface morphology of the Ni films electrodeposited by the PVM at 90 °C with  $U_{\text{pos}} = -1.0$  V and  $f = 0.05$  kHz. (a, b)  $\nu = 10\%$ , (c, d)  $\nu = 30\%$ , and (e, f)  $\nu = 50\%$ .

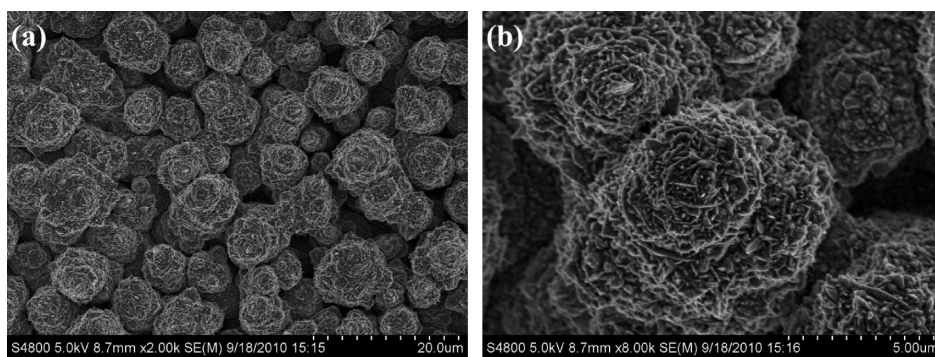


**Figure 4.** SEM image of the Ni film electrodeposited by the RVM at 90 °C. (a) Low magnification, (b) high magnification.

patterns and are ready to disperse on the cell structures randomly, as shown in Figure 3e and f. In this case, the Ni bubbles with the size of 20–50 nm are grown on the 300–500 nm sized cells. The present investigation indicates that a lower duty cycle favors the formation of aligned patterns of

deposits, which should be attributed to the more off-time of plating allowing the Ni adatoms have enough time to move to look for the lowest energy sites. However, a relatively higher duty cycle would make the adatoms have no time to arrange their sites, and hence, the films exhibit the random appearance. The extreme

case for the higher duty cycle should be the constant voltage electrodeposition mode. It should be noted that the Ni

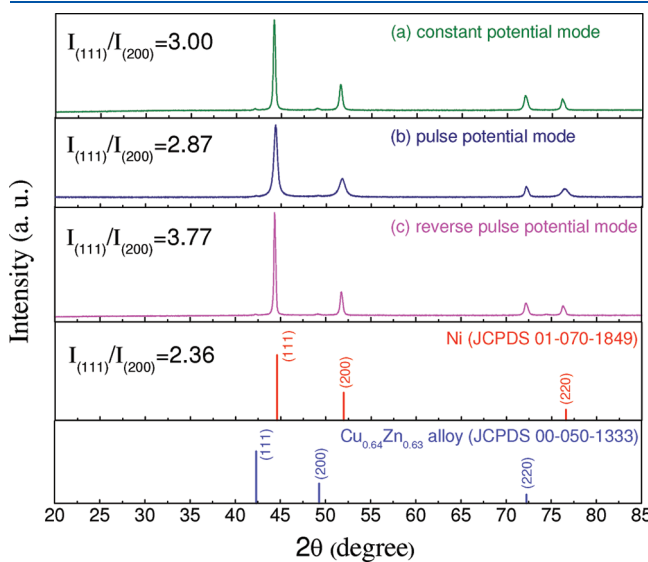


**Figure 5.** Typical XRD patterns of the as-deposited Ni films on the brass substrate. Samples (a), (b), and (c) correspond to those as shown in Figures 2a, 3a, and 4, respectively.

nanostructures shown in Figure 3 have not been observed before and the formation mechanism is not clear now. However, a synergistic effect from the EDS and the applied voltage profiles might be suggested as being responsible for the formation of micro/nanobinary Ni structures.

The reverse pulse electrodeposition is generally adopted to deposit metals with fine microstructures,<sup>24</sup> in which the reverse current would remove deposits from existing locations and make the metal distribution more uniform. In this study, we also give a preliminary investigation on the reverse pulse voltage electrodeposition in DES-based electrolytes, which is expected to shed light on tailoring the architecture of metals on micro/nanoscales in ionic liquids. Figure 4 shows the SEM image of the as-deposited Ni film by the RVM at the bath temperature of 90 °C. The flower-like Ni film with 5–10 μm sized clusters can be observed, which possesses remarkable hierarchical structures sprawling to several generations with apparent self-similarity, as shown in Figure 4b. Moreover, the structure of the Ni flowers is also composed by Ni nanosheets as shown in Figures 2 and 3, which indicates that the RVM electrodeposition is an effective method to control over the topography of the deposits in ionic liquids.

**3.2. XRD and TEM Analysis.** Figure 5 gives the typical XRD patterns of the electrodeposited Ni films as shown in Figures 2a, 3a, and 4. As we can see, the peaks at 44.6°, 51.9°, and 76.5° are assigned to the face-centered cubic (fcc) Ni planes of (111),

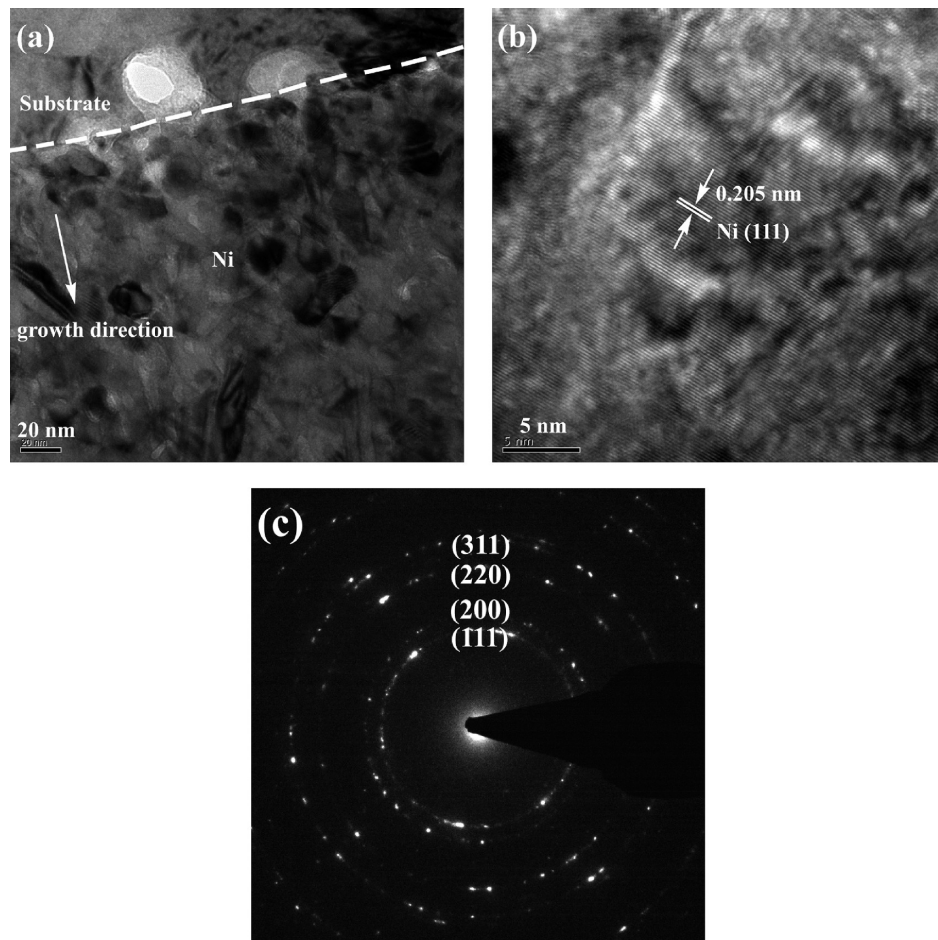


**Figure 6.** Cross-sectional TEM micrograph of the Ni film electrodeposited by the CVM at 90 °C. (a) TEM image of the Ni/brass interface, where the growth direction of Ni film is indicated by the arrow. (b) HR-TEM image of the Ni grains. (c) SAD patterns corresponding to the Ni film.

(200), and (220), respectively, which well agrees with the report of JCPDS 01-070-1849. The other peaks shown in Figure 5 can be assigned to the brass substrate, Cu<sub>0.64</sub>Zn<sub>0.63</sub> alloy (JCPDS 00-050-1333). Recently, Lahiri and Das found that hexagonal close packed (hcp) structured Ni could be electrodeposited from NiCl<sub>2</sub>-1-ethyl-3-methylimidazolium chloride ionic liquid at 150 °C, which was attributed to the deposition temperature and H<sup>+</sup> ions in the ionic liquid.<sup>25</sup> In this study, no other Ni phase is detected by the XRD analysis. Furthermore, for the three samples, the peak intensity ratios of the (111) to (200) diffractions,  $I_{(111)}/I_{(200)}$ , are all higher than that from a polycrystalline Ni with randomly distributed grains, as indicated in Figure 5. Surface energies associated with different crystallographic planes are usually

different, and the general sequence  $\gamma_{\{111\}} < \gamma_{\{100\}} < \gamma_{\{110\}}$  holds for most fcc crystals.<sup>4,26</sup> The XRD results indicate that the {111} plane of the electrodeposited Ni with lower surface energy compared to the other planes is preferentially oriented parallel to the surface of the supporting substrate.

As a representative case of study, the following characterizations were mainly focused on the Ni nanosheet films (Figure 2a) electrodeposited by the CVM at 90 °C, unless otherwise stated. Figure 6 shows the cross-sectional TEM micrograph of the CVM electrodeposited Ni film on the brass substrate. As shown in Figure 6a, the interface of the substrate and Ni film can be clearly distinguished, which is also highlighted by a dashed line. The substrate has a coarse grain structure, and the Ni film has a nanocrystalline structure with an average grain size of about 30 nm. No obvious pores or defects are found in the Ni film. Figure 6b gives the HR-TEM image of the Ni grains, where the plane fringe with 0.205 nm crystalline plane spacing can be assigned to the Ni {111} plane. Moreover, the ringlike patterns of the selected area diffraction (SAD) also confirm the nanocrystallite structure of the Ni film, as shown in Figure 6c. The SAD patterns also indicate the fcc structure of the Ni deposit, which is in good agreement with the result of XRD.

**3.3. Surface Structure.** The XPS analysis is carried out to investigate the surface structure of the Ni film as shown in Figure 2a, and the XPS results are shown in Figure 7. The binding energies in the XPS spectra are calibrated by using that of C 1s (284.8 eV). All peaks in the XPS full spectrum shown in Figure 7a can be ascribed to Ni, C, and O elements. The presence of C comes mainly from pump oil in the vacuum system of the XPS equipment. The presence of O is consistent with the EDS analysis shown in Figure 2c. The high resolution spectra for Ni is shown in Figure 7b, where the peak center at 852.2 and 869.6 eV can be assigned to Ni 2p<sub>3/2</sub> and Ni 2p<sub>1/2</sub>, respectively. There is a small peak that can be found at 860.9 eV, which might be assigned to the NiO.<sup>27</sup> The formation of NiO may be attributed to the high activity of the nanocrystalline Ni structures.

**3.4. Wettability and Corrosion Property.** As shown in Figures 2, 3, and 4, various micro/nanobinary structures of Ni films have been fabricated by the programmed electrodeposition from the DES at a high temperature. It is even more miraculous to find that some of those Ni films exhibit superhydrophobic surfaces at their as-deposited state, giving the water contact angles close to or higher than 160° as shown in Table 1. The roughness of the substrate is 0.074 μm,<sup>22</sup> which is similar to that of the smooth Ni film electrodeposited by the CVM at room temperature (Figure 2d). Thus, the similar wetting behavior is

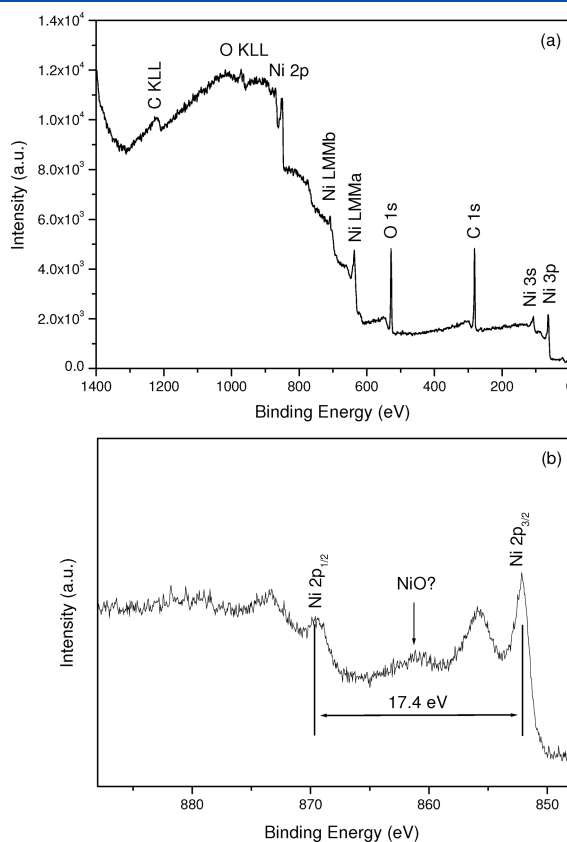


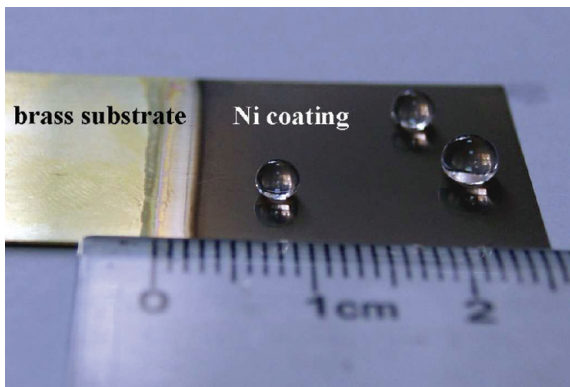
Figure 7. (a) XPS full spectrum of the Ni film electrodeposited by the CVM at 90 °C. (b) High-resolution spectra for Ni species.

Table 1. Summary of CA Measurements of the Ni Films Fabricated in This Study and the Substrate

Samples	Figure 2a and 2b	Figure 2d	Figure 2e
Contact angle	CA=164±1°	CA=105±1°	CA=130±3°
Samples	Figure 3 <sup>a</sup>	Figure 4	Substrate
Contact angle	v = 10% CA=152±1°	CA=115±5°	CA=98±2°

<sup>a</sup> All samples as shown in Figure 3 give the similar CA values ranging from 150° to 155°.

observed in the smooth Ni film and the substrate. However, the CA value of the Ni film electrodeposited by the CVM at 60° increases to about 130° due to its relatively high surface roughness. As shown in Figure 8, the approximately spherical geometry of the water droplet can be formed when the water droplets are deposited on the Ni film electrodeposited by the CVM at 90°, thus giving a CA value of about 164° (Table 1). The tilt angle reflects the difference between the advancing and the receding contact angles. The measurement shows that the tilt angle of the Ni film electrodeposited by the CVM at 90° is lower than 3° (see Supporting Information Movie 1S). The low tilt angle indicates that the water droplet can easily roll down on the surface when it tilts. Moreover, as shown in Figure 9a and b, the Ni film electrodeposited by the CVM at 90° has almost the same value of the advancing and receding angles ( $\theta_a = 166^\circ$  vs  $\theta_r = 162^\circ$ );



**Figure 8.** Photograph of water droplets on the Ni film surface fabricated by the CVM electrodeposition at 90 °C.

thus, the contact angle hysteresis ( $\Delta\theta$ ) is about 4°. We also found that all samples electrodeposited by the PVM exhibit similar CA values ranging from 150° to 155° (see Table 1) but a higher  $\Delta\theta$  of about 55° as shown in Figure 9. However, the Ni sample electrodeposited by the RVM possesses an unstable CA value of  $115 \pm 5^\circ$  (Table 1), which should be related to its micrometer-scaled surface topography as shown in Figure 4. Therefore, the surface morphology with a vast number of supporting points within nanoscales, just as shown in Figure 2a and b, plays an important role in the achievement of a superhydrophobic Ni surface without any further chemical modification.

In the literature, for example,<sup>4–10,28–30</sup> the pure metal is hydrophilic in nature and the superhydrophobic pure metal surfaces are usually fabricated by the two-step approaches, that is, the creation of micro/nanobinary structures followed by a surface treatment via low surface free energy materials. Here, we demonstrate a novel one-step approach to get the superhydrophobic metal surfaces. Based on the above analysis, we suggest two possible reasons for the unconventional wettability of Ni films. One should be attributed to the appropriate surface roughness accompanied with vigorous nanoscaled structures, for example, as shown in Figure 2a and b. The other might be the chemical composition caused by oxygen on the film surface, which is revealed by EDS and XPS analysis. Nevertheless, the mechanism underlying the abnormal wettability of the electrodeposited Ni films is not clear now, and it is really an open question that deserves further investigation.

The open circuit potentials (OCP) of the brass substrate and the superhydrophobic Ni film electrodeposited by the CVM at 90 °C were measured in 3 wt % NaCl solution and shown in Figure 10a. For the brass substrate, the OCP is stable around  $-0.215$  V even after 100 min of immersion. However, the OCP

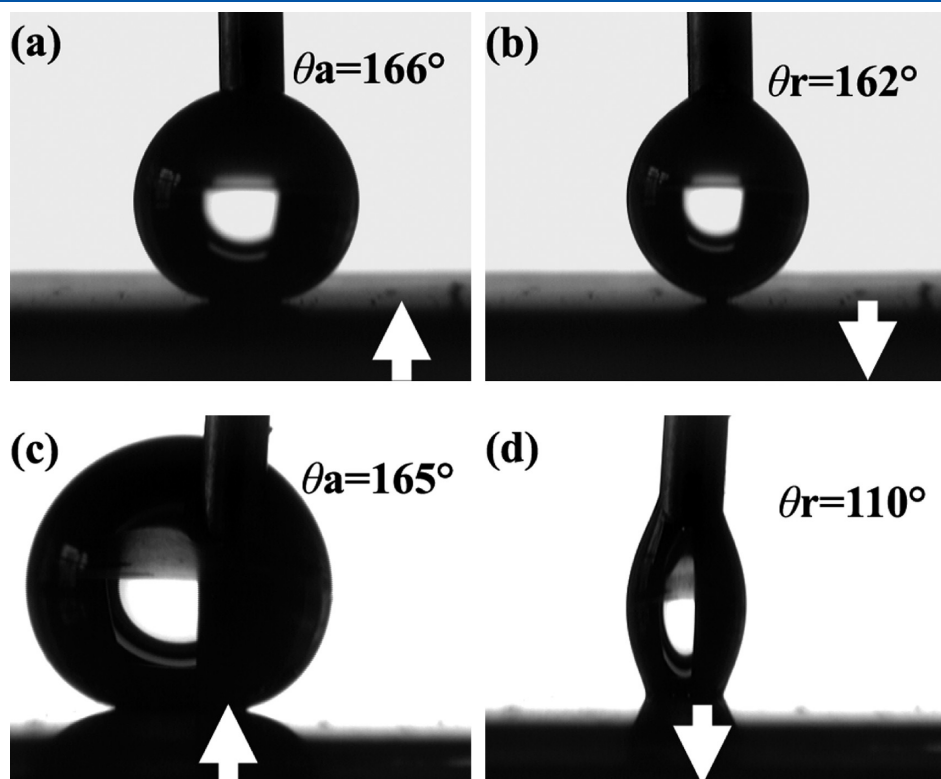


**Figure 9.** Contact angle hysteresis measurements of the Ni film electrodeposited at 90 °C by the (a, b) CVM and (c, d) the PVM.

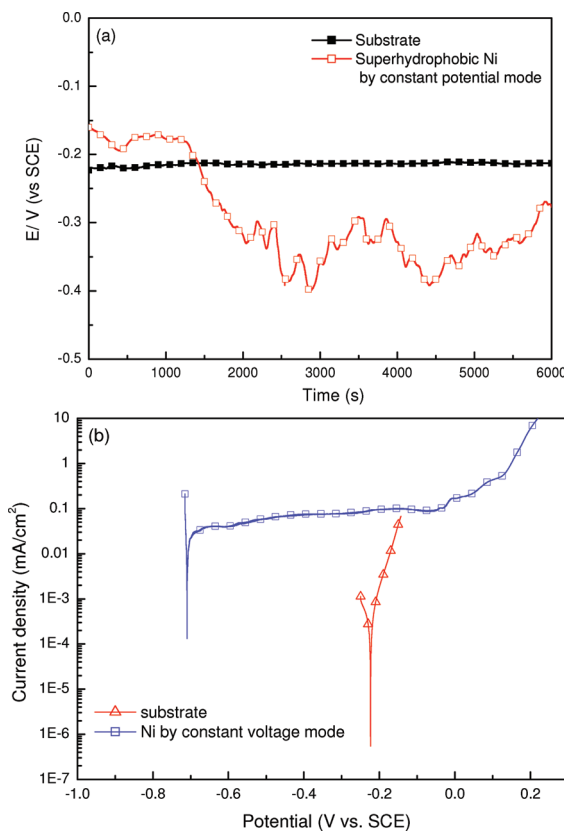


**Figure 10.** (a) Measured open circuit potentials and (b) electrochemical polarization curves of the brass substrate and the superhydrophobic Ni film electrodeposited by the CVM at 90 °C.

of the superhydrophobic Ni film fluctuates and is in the range of  $-0.393$  to  $-0.173$  V during the immersion process, which is near to the OCP of the substrate. Figure 10b gives the electrochemical polarization curves for the brass substrate and the superhydrophobic Ni film electrodeposited by the CVM at 90 °C. The cathodic reaction in the polarization curves corresponds to the evolution of the hydrogen. The anodic branch of the polarization curve has the most important features related to the corrosion resistance. For the brass substrate, when the applied potential increases into the anodic region, an activation-controlled anodic process is observed. The polarization current increases with increasing the applied anodic potential, and no obvious passivation occurs. The brass substrate possesses a corrosion potential  $E_{corr}$  of about  $-0.225$  V, which is consistent with the measured OCP. However, for the superhydrophobic Ni film, the  $E_{corr}$  values decrease to  $-0.710$  V much lower than its OCP, which is also largely negative to the  $E_{corr}$  of substrate. Moreover, for the Ni film, between the potential values of  $-0.660$  and  $-0.032$  V, the passivation phenomenon is clearly observed as the formation of a thin passive film occurs, resulting in a constant current at approximately  $0.070$  mA/cm $^2$ . Therefore, the superhydrophobicity of the Ni films is expected to provide high corrosion resistance for the substrate in the aqueous solutions.

#### 4. CONCLUSION

In this study, we demonstrate that programmed electrodeposition is an effective method to manipulate the micro/nano-architectures of Ni films from a ChCl-based ionic liquid. A variety

of fcc Ni nanostructures, such as nanosheets, aligned nanostrips, and hierarchical flowers, were successfully electrodeposited via control of deposition voltage profiles, bath temperatures, and duty cycles. It is surprisingly found that that the as-deposited Ni films exhibit superhydrophobic surfaces without any further modifications by the low surface energy materials, which leads us for the first time to report one-step methods to fabricate superhydrophobic Ni surfaces. Moreover, the superhydrophobic Ni film exhibits the obvious passivation and relatively lower corrosion potential during the electrochemical measurements. This study indicates that electrochemical deposition in ionic liquids would offer much more opportunities for the manipulation of nanostructures of metals and alloys.

#### ■ ASSOCIATED CONTENT

**S Supporting Information.** Movie 1S showing that the tilt angle of the Ni film electrodeposited by the CVM at 90° is lower than 3°. This material is available free of charge via the Internet at <http://pubs.acs.org>.

#### ■ AUTHOR INFORMATION

##### Corresponding Author

\*E-mail: changdong\_gu@hotmail.com; cdgu@zju.edu.cn. Telephone/fax: +86 571 87952573.

#### ■ ACKNOWLEDGMENT

The work was supported by the National Natural Science Foundation of China (51001089), the Specialized Research Fund for the Doctoral Program of Higher Education of China (2010-0101120026), the Research Foundation of Education Bureau of Zhejiang Province (Y200906938), and the Fundamental Research Funds for the Central Universities (2009QNA4006).

#### ■ REFERENCES

- (1) Zhang, X.; Shi, F.; Niu, J.; Jiang, Y. G.; Wang, Z. Q. *J. Mater. Chem.* **2008**, *18*, 621–633.
- (2) Sun, T. L.; Feng, L.; Gao, X. F.; Jiang, L. *Acc. Chem. Res.* **2005**, *38*, 644–652.
- (3) Barthlott, W.; Neinhuis, C. *Planta* **1997**, *202*, 1–8.
- (4) Gu, C. D.; Zhang, T. Y. *Langmuir* **2008**, *24*, 12010–12016.
- (5) Gu, C. D.; Ren, H.; Tu, J. P.; Zhang, T. Y. *Langmuir* **2009**, *25*, 12299–12307.
- (6) Shi, F.; Song, Y. Y.; Niu, H.; Xia, X. H.; Wang, Z. Q.; Zhang, X. *Chem. Mater.* **2006**, *18*, 1365–1368.
- (7) Gu, C. D.; Xu, X. J.; Tu, J. P. *J. Phys. Chem. C* **2010**, *114*, 13614–13619.
- (8) Xu, X. H.; Zhang, Z. Z.; Yang, J. *Langmuir* **2010**, *26*, 3654–3658.
- (9) Gu, C. D.; Zhang, J.; Tu, J. P. *J. Colloid Interface Sci.* **2010**, *352*, 573–579.
- (10) Shafei, M.; Alpas, A. T. *Appl. Surf. Sci.* **2009**, *256*, 710–719.
- (11) Cao, Z. W.; Xiao, D. B.; Kang, L. T.; Wang, Z. L.; Zhang, S. X.; Ma, Y.; Fu, H. B.; Yao, J. N. *Chem. Commun.* **2008**, 2692–2694.
- (12) Armand, M.; Endres, F.; MacFarlane, D. R.; Ohno, H.; Scrosati, B. *Nat. Mater.* **2009**, *8*, 621–629.
- (13) Endres, F. *Chem. Phys. Chem* **2002**, *3*, 144–154.
- (14) El Abedin, S. Z.; Moustafa, E. M.; Hempelmann, R.; Natter, H.; Endres, F. *Chem. Phys. Chem* **2006**, *7*, 1535–1543.
- (15) Endres, F.; Bukowski, M.; Hempelmann, R.; Natter, H. *Angew. Chem., Int. Ed.* **2003**, *42*, 3428–3430.
- (16) Abbott, A. P.; Boothby, D.; Capper, G.; Davies, D. L.; Rasheed, R. K. *J. Am. Chem. Soc.* **2004**, *126*, 9142–9147.

- (17) Abbott, A. P.; Ryder, K. S.; Konig, U. *Trans. Inst. Met. Finish.* **2008**, *86*, 196–204.
- (18) Gu, C.; Lian, J.; He, J.; Jiang, Z.; Jiang, Q. *Surf. Coat. Technol.* **2006**, *200*, 5413–5418.
- (19) Gu, C.; Lian, J.; Jiang, Z.; Jiang, Q. *Scr. Mater.* **2006**, *54*, 579–584.
- (20) Abbott, A. P.; El Ttaib, K.; Ryder, K. S.; Smith, E. L. *Trans. Inst. Met. Finish.* **2008**, *86*, 234–240.
- (21) Gou, S.-P.; Sun, I. W. *Electrochim. Acta* **2008**, *53*, 2538–2544.
- (22) Gu, C. D.; You, Y. H.; Yu, Y. L.; Qu, S. X.; Tu, J. P. *Surf. Coat. Technol.* **2011**, *205*, 4928–4933.
- (23) Abbott, A. P.; Capper, G.; Davies, D. L.; Rasheed, R. K.; Shikotra, P. *Inorg. Chem.* **2005**, *44*, 6497–6499.
- (24) Gu, C. D.; Xu, H.; Zhang, T. Y. *J. Micromech. Microeng.* **2009**, *19*, 065011.
- (25) Lahiri, A.; Das, R. *J. Appl. Electrochem.* **2010**, *40*, 1991–1995.
- (26) Wang, Z. L. *J. Phys. Chem. B* **2000**, *104*, 1153–1175.
- (27) Chastain, J.; Moulder, J. F. *Handbook of x-ray photoelectron spectroscopy:a reference book of standard spectra for identification and interpretation of XPS data*; Physical Electronics Division, Perkin-Elmer Corp.: Eden Prairie, MN, 1992.
- (28) Yao, X.; Xu, L.; Jiang, L. *Adv. Funct. Mater.* **2010**, *20*, 3343–3349.
- (29) Gu, C. D.; Tu, J. P.; Zhang, T. Y. *Appl. Surf. Sci.* **2010**, *257*, 1779–1785.
- (30) Ye, W.; Yan, J.; Ye, Q.; Zhou, F. *J. Phys. Chem. C* **2010**, *114*, 15617–15624.